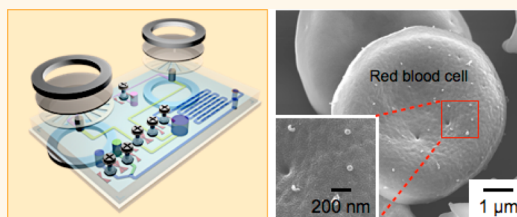


# Magnetic Nanosensor for Detection and Profiling of Erythrocyte-Derived Microvesicles

Junsung Rho,<sup>†,‡</sup> Jaehoon Chung,<sup>†,‡</sup> Hyungsoon Im,<sup>†</sup> Monty Liong,<sup>†</sup> Huilin Shao,<sup>†</sup> Cesar M. Castro,<sup>†,‡</sup> Ralph Weissleder,<sup>†,§</sup> and Hakho Lee<sup>†,\*</sup>

<sup>†</sup>Center for Systems Biology, Massachusetts General Hospital, 185 Cambridge Street, CPZN 5206, Boston, Massachusetts 02114, United States, <sup>‡</sup>Massachusetts General Hospital Cancer Center, 55 Fruit Street, Boston, Massachusetts 02114, United States, and <sup>§</sup>Department of Systems Biology, Harvard Medical School, Boston, Massachusetts 02115, United States. <sup>‡</sup>These authors contributed equally.

**ABSTRACT** During the course of their lifespan, erythrocytes actively shed phospholipid-bound microvesicles (MVs). In stored blood, the number of these erythrocyte-derived MVs has been observed to increase over time, suggesting their potential value as a quality metric for blood products. The lack of sensitive, standardized MV assays, however, poses a significant barrier to implementing MV analyses into clinical settings. Here, we report on a new nanotechnology platform capable of rapid and sensitive MV detection in packed red blood cell (pRBC) units. A filter-assisted microfluidic device was designed to enrich MVs directly from pRBC units, and label them with target-specific magnetic nanoparticles. Subsequent detection using a miniaturized nuclear magnetic resonance system enabled accurate MV quantification as well as the detection of key molecular markers (CD44, CD47, CD55). When the developed platform was applied, MVs in stored blood units could also be monitored longitudinally. Our results showed that MV counts increase over time and, thus, could serve as an effective metric of blood aging. Furthermore, our studies found that MVs have the capacity to generate oxidative stress and consume nitric oxide. By advancing our understanding of MV biology, we expect that the developed platform will lead to improved blood product quality and transfusion safety.



**KEYWORDS:** nanotechnology · biosensor · microvesicles · microfluidics · blood · transfusion

Circulating microvesicles (MVs) are small phospholipid vesicles, released into the bloodstream by virtually all eukaryotic cell types, including erythrocytes, platelets, leukocytes and endothelial cells.<sup>1</sup> Initially underappreciated as cellular “dusts”,<sup>2</sup> MVs have more recently been recognized to play vital biological functions, including the facilitation of cell-to-cell interactions, induction of cell signaling and even the transferral of genetic material between different cell types.<sup>3–5</sup> In particular, recent studies have established an integral role for microvesiculation in erythrocyte aging processes.<sup>6</sup> By shedding MVs, erythrocytes eliminate toxic, denatured hemoglobin as well as membrane proteins, which would otherwise lead to early phagocytosis.<sup>7</sup> In stored blood, this process leads to an increase in erythrocyte-derived MVs over time, which suggests that MVs could be potentially used as an indicator of blood product quality.<sup>8</sup> Such applications could

have significant clinical implications, considering the growing evidence of transfusion complications associated with aging blood products (e.g., multiple organ failure,<sup>9,10</sup> increased mortality in critically ill patients,<sup>11</sup> postoperative complications after cardiac surgery<sup>12</sup>).

The lack of sensitive, standardized MV assays poses a significant barrier to implementing MV analyses in routine clinical settings.<sup>13,14</sup> Flow cytometry has been the method of choice for analyzing MVs due to its high throughput and molecular detection capabilities.<sup>15</sup> Yet, the detection is limited by weak light scattering, because MVs are smaller than the wavelength of light. As a result, flow cytometry measurements severely underestimate total MV counts. Newer counting approaches based on particle-tracking or dynamic light scattering now offer much more accurate MV counts, approximately  $10^3$ -fold higher than those reported by flow cytometry.<sup>16</sup> However,

\* Address correspondence to hlee@mg.harvard.edu.

Received for review September 26, 2013 and accepted November 26, 2013.

Published online December 02, 2013  
10.1021/nn405016y

© 2013 American Chemical Society

these methods are unable to provide molecular information on MVs. While conventional protein analyses such as Western blotting and enzyme-linked immunosorbent assays (ELISA) can provide such information, they generally require large numbers of MVs and involve time-consuming isolation processes. To translate MV analyses to routine clinical practice and blood banking, the prevailing challenge is developing simpler and more sensitive sensing technologies.

We herein report on the development of a new nanotechnology platform capable of accurate and rapid MV analyses. The system incorporates both microfluidics and magnetic sensing technologies. A microfluidic cartridge directly isolates MVs from blood before labeling them with magnetic nanoparticles (MNPs). The labeled MVs are then detected by a miniaturized micronuclear magnetic resonance ( $\mu$ NMR) system.<sup>17</sup> Processing of an entire sample is performed within the chip, obviating the need for external MV isolation steps (e.g., ultracentrifugation<sup>18</sup>). Furthermore, because the assay requires only small volumes of blood (<200  $\mu$ L), it is possible to monitor a given blood product both repeatedly and sequentially. Using the developed platform, we measured MV concentrations as well as MV proteins. Moreover, in a longitudinal study, we found that increased MV counts corresponded with prolonged storage. The protein profile per vesicle, however, displayed negligible changes, indicating an increase of a homogeneous MV population during blood aging. Importantly, MVs were found to contain hemoglobin molecules that exhibit the same capacity for peroxidase-like activity and nitric oxide depletion as cell-free hemoglobin; these findings may help explain the adverse effects often seen in clinical settings with older blood units. On the basis of these findings, we identified erythrocyte-derived MVs as an effective biomarker for monitoring blood product quality.

## RESULTS

**Assay Platform and Principle.** Scanning electron microscopy revealed the presence of budding MVs (<200 nm) on the surface of erythrocytes (Figure 1A). To enable reliable detection of such small objects, we used polymer microbeads as a solid support for magnetic targeting (Figure 1B). Namely, MVs were first captured on antibody-coated microbeads (diameter, 1  $\mu$ m) and subsequently labeled with MNPs *via* secondary antibodies. MNPs and secondary antibodies were modified with tetrazine (TZ) and *trans*-cyclooctene (TCO), respectively. The fast, covalent cycloaddition between TZ and TCO maximized MNP binding to target MV proteins, and thus served to improve overall detection sensitivity.<sup>19,20</sup> The amount of MNPs was then quantified by measuring the transverse relaxation rate ( $R_2$ ) of samples by  $\mu$ NMR; the  $R_2$  value displays a linear increase with MNP concentration, enabling quantitative molecular analyses.<sup>21,22</sup> The bead-based  $\mu$ NMR detection significantly simplified the assay, as conventional centrifugation or filtration can be

used to wash excess reagents. It also showed improved detection sensitivity, compared to the magnetic relaxation switching assay,<sup>22</sup> since no free-floating MNPs are present in the background.

To facilitate the developed assay procedure, a microfluidic cartridge was implemented for on-chip MV isolation and labeling. This chip uses membrane filters, which size-selectively isolate MVs from unprocessed blood samples (Figure 1C). A capillary layer, inserted underneath the membrane, guides the filtered MVs to the collection channel. The filter and guiding layer are sandwiched between two permanent ring-magnets, which enable easy replacement of filter units when processing large volumes of samples. The size cutoff for the membrane filter is  $\sim$ 1  $\mu$ m (Figure S1). The collected MVs are subsequently captured onto beads and labeled with MNPs (see Experimental Section and Figure S2 for details). To provide on-chip processing, we also integrated a microfluidic mixer for fast in-flow conjugation, an in-line filter (pore size: 400 nm) to collect microbeads (1  $\mu$ m), and torque-assisted valves for fluidic control (Figure 1D).

Figure 1E shows a photograph of a prototype device. This system can filter 300  $\mu$ L (150  $\mu$ L per inlet) of packed red blood cell (pRBC) samples in less than 10 min. Nanoparticle tracking analysis (NTA) of the purified MVs revealed a single population with an average size of 167 nm (Figure 1F); this size was consistent with electron microscopy measurements (Figure 1A), and corroborated a likely limitation of detecting MVs with flow cytometry. The collected MVs were then bead-captured and magnetically labeled on-chip (Figure 1G). The entire assay took less than 30 min, and thus allowed for real-time analysis of blood samples.  $\mu$ NMR measurements of pRBC samples processed by the microfluidic device were also found to be identical to measurements of samples prepared by ultracentrifugation. This confirmed that the microfluidic device can enrich MVs, and that other proteins in the stored blood supernatant have minimal effect on  $\mu$ NMR measurements.

**Assay Optimization: MV Counting and Profiling.** We first optimized the assay platform for quantitative MV analyses. To measure MV concentration ([MV]), we chose to target CD235a (Glycophorin A), an abundant protein marker for erythrocytes.<sup>23</sup> Samples were prepared from pRBC units. MVs are first captured on microbeads coated with CD235a antibodies, and subsequently labeled with MNPs for CD235a. For a given [MV], we changed the bead concentration to achieve the maximal  $R_2$  values; the optimal ratio between bead and MV concentrations was found to be  $\sim$ 1:20. The measured  $R_2$  values ( $\Delta R_2^{\text{CD235a}}$ ) were linearly proportional to [MV], which was independently estimated by NTA (Figure 2A). Similar measurements on CD235a expression by ELISA and  $\mu$ NMR likewise showed excellent correlations (Figure 2B). Importantly, the  $\Delta R_2^{\text{CD235a}}$

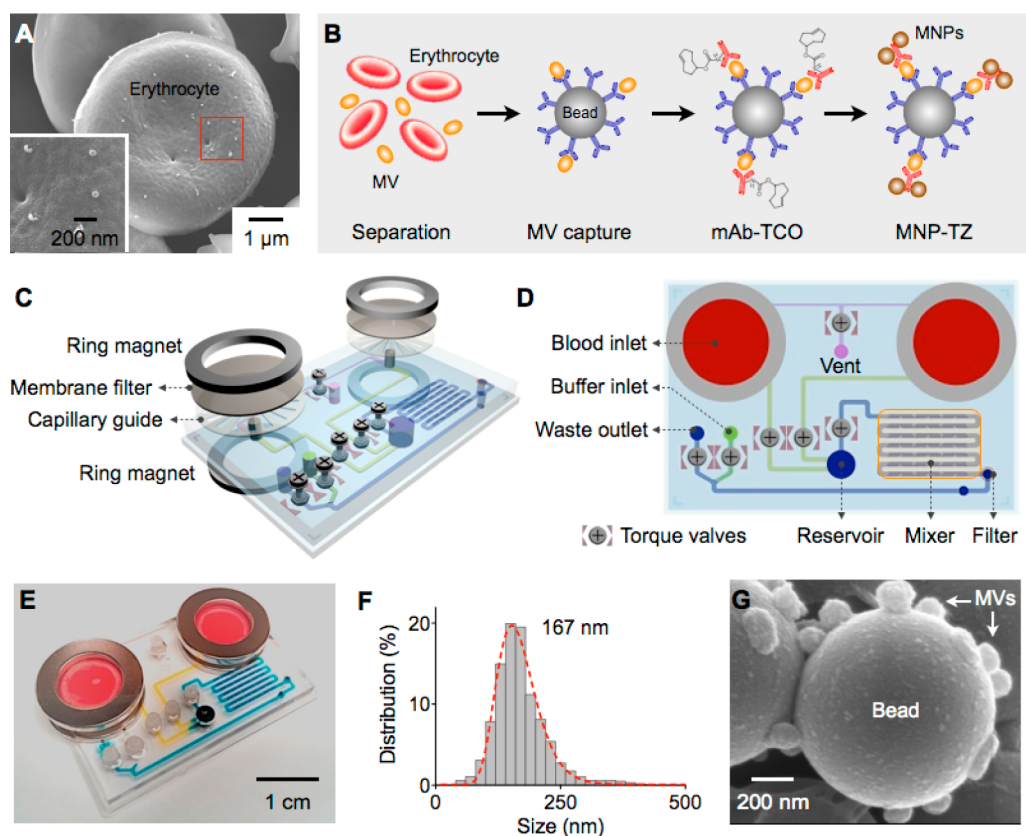


**Figure 1.** System design and assay schematic. (A) A scanning electron micrograph of an erythrocyte with budding microvesicles (MVs; inset) from a packed red blood cell unit (pRBC; storage day, 34). (B) A scheme of the assay design: MVs are separated from blood, and captured by antibody-coated microbeads (1  $\mu\text{m}$  in diameter). Immunomagnetic labeling subsequently renders the beads superparamagnetic. The cycloaddition reaction between *trans*-cyclooctene (TCO) and tetrazine (TZ) is employed to couple the magnetic nanoparticles (MNPs) to antibodies (mAbs). (C) This exploded view of the  $\mu\text{NMR}$  system shows how the membrane filter and capillary guide are sandwiched between two ring magnets. The filter set can thus be easily replaced when large volumes of samples are processed. (D) The device consists of two inlets for blood loading, torque-assisted valves for fluidic control, a herringbone mixer, and an embedded filter for microbead capture. MVs are collected into the reservoir, after which other reagents (microbeads, mAb-TCO, MNP-TZ) are serially loaded (see Supporting Information for device operation). (E) A photograph of a prototype device. The device measures  $76 \times 52 \text{ mm}^2$ , and can filter  $300 \mu\text{L}$  ( $150 \mu\text{L}$  per inlet) of pRBCs from a single sample load. (F) The size distribution of filtered MVs analyzed by nanoparticle tracking analysis (NTA). The average size of MVs was 167 nm. (G) Following labeling with the developed microfluidic device, MVs were effectively captured by microbeads, as confirmed by electron microscopy.

values, normalized against [MV], were all statistically identical ( $P > 0.44$ , one-way ANOVA) across the different pRBC units (Figure 2C); these findings established  $\Delta R_2^{\text{CD}235}$  as a good metric for estimating erythrocyte-derived MV counts. The detection sensitivity of measurements by  $\mu\text{NMR}$  was  $\sim 2 \times 10^6 \text{ MV}/\mu\text{L}$ , and the dynamic range was up to  $\sim 2 \times 10^8 \text{ MV}/\mu\text{L}$  (Figure S3). Note that the typical [MV] in stored pRBC units was in the range of  $10^8$  to  $10^9 \text{ MV}/\mu\text{L}$ . Serial and multiple assays on a given pRBC unit could thus be performed with minimal sample consumption.

We subsequently profiled other protein markers, each selected for their prevalence and potential significance to erythrocyte biology. Three representative markers were screened: (i) CD44, an adhesion receptor implicated in the adhesion of lymphocytes and monocytes to endothelial cells in the sickle cell disease model;<sup>24</sup> (ii) CD47, a marker of self on erythrocytes, whose decrease leads to phagocytosis of senescent

erythrocytes;<sup>25,26</sup> and (iii) CD55, a well-known erythrocyte transmembrane glycoprotein complement regulator involved in paroxysmal nocturnal hemoglobinuria. For each pRBC unit, we separately measured  $\Delta R_2^{\text{CD}235\text{a}}$  and  $\Delta R_2^{\text{mAb}}$ , where  $\Delta R_2^{\text{mAb}}$  is the  $R_2$  changes associated with a target biomarker. We then defined  $\xi^{\text{mAb}} (= R_2^{\text{mAb}}/\Delta R_2^{\text{CD}235\text{a}})$  to report the microvesicular expression of a target marker. With  $\Delta R_2^{\text{CD}235\text{a}}$  functioning as a metric for [MV],  $\xi^{\text{mAb}}$  is independent of variations in MV quantity between different samples. With the microfluidic platform, we could reliably screen MVs for target markers using small sample volumes ( $10 \mu\text{L}$ ). Importantly,  $\mu\text{NMR}$  measurements for each marker showed excellent correlations ( $R^2 > 99\%$ ) with corresponding ELISA measurements (Figure 2D).

**Temporal Changes of MVs in Stored Blood.** In aging erythrocytes, [MV] was observed to increase in stored pRBC units, as estimated by  $\Delta R_2^{\text{CD}235\text{a}}$  measurements (Figure S4A). The ratio between  $R_2^{\text{CD}235\text{a}}$  and [MV],

however, remained unchanged over time ( $P > 0.43$ , one-way ANOVA; Figure 3A). The increase in  $\Delta R_2^{\text{CD235a}}$  could thus be attributed to the increase in MV counts, not to the change in CD235a expression on individual MVs. The expression levels of surface markers also showed negligible changes over their initial values

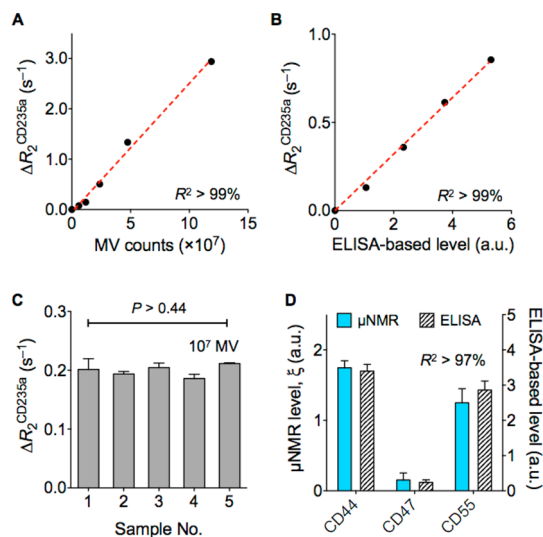


**Figure 2.** Validation of the micronuclear magnetic resonance ( $\mu\text{NMR}$ ) assay. (A) MVs were magnetically labeled by targeting CD235a, an abundant protein present on the human erythrocyte membrane. Labeled MVs were then subjected to  $\mu\text{NMR}$  detection (sample volume,  $1 \mu\text{L}$ ). The measured relaxation rate ( $R_2$ ) showed an excellent linear correlation ( $R^2 > 99\%$ ) with MV numbers (estimated by NTA). (B) The analytical capacity of  $\mu\text{NMR}$  detection was further verified by fluorescent-based ELISA (CD235a). (C) When normalized against MV counts, the  $R_2$  values associated with CD235a ( $\Delta R_2^{\text{CD235a}}$ ) were statistically identical ( $P > 0.44$ ) for different blood samples. Thus,  $\Delta R_2^{\text{CD235a}}$  could be used as a universal measure of erythrocyte-derived MVs. (D) The microvesicular expression level ( $\xi$ ) of a target marker was defined as the ratio between  $\Delta R_2$  for the target marker and  $\Delta R_2^{\text{CD235a}}$ . Three erythrocyte surface markers (CD44, CD47, CD55) were profiled via  $\mu\text{NMR}$ . The measured  $\xi$  profiles corresponded well with screening results obtained by ELISA ( $R^2 > 97\%$ ).

(Figure 3B). These findings strongly suggest that highly homogeneous MVs are formed with blood aging. Consistent with this model, the median size of the MVs (estimated by NTA) also remained unchanged for the duration of storage (Figure S4B).

We next went on to monitor multiple pRBC units ( $n = 7$ ) longitudinally, measuring [MV] via  $R_2^{\text{CD235a}}$ . All the samples showed a linear increase in [MV] with time ( $P < 0.002$ , mixed model; Figure 3C). Interestingly, the initial [MV] value and its subsequent rise were highly variable among samples. For instance, some pRBC units exhibited higher [MV] values even in the early days of storage compared to other units after  $\sim 40$  days (Figure 3C). This highlights the importance of monitoring individual blood units serially to evaluate their quality, rather than relying on days of storage as the sole indicator.

**MVs Retain Toxicities of Cell-Free Hemoglobin.** Cell-free hemoglobin (Hgb) that is not encapsulated within an intact cell membrane could damage vascular systems in transfused hosts by generating reactive oxygen species (ROS) as well as by scavenging a critical vasodilator, nitric oxide (NO).<sup>27–29</sup> Studies have shown adverse effects of plasma hemoglobin, released from hemolysis, in various disease states.<sup>30,31</sup> However, it remains unclear whether hemoglobin encapsulated within MVs retain similar toxicities to cell-free hemoglobin.

To address this question, we first quantified the Hgb content of MVs. Stored blood samples were processed using the developed microfluidic cartridge, and Hgb concentrations were measured (see Experimental Section for details). The average Hgb contents per MV was measured to be  $1.5 \times 10^{-15}$  g (Figure 4A). The total amount of MV-derived Hgb increased with storage time as more MVs were formed with blood aging. We next examined whether MV-derived Hgb can generate oxidative stress. Since heme, an integral part of Hgb, is an active element of horseradish peroxidase (HRP), we hypothesized that 3,3',5,5'-tetramethylbenzidine (TMB), which is a commonly used colorimetric substrate

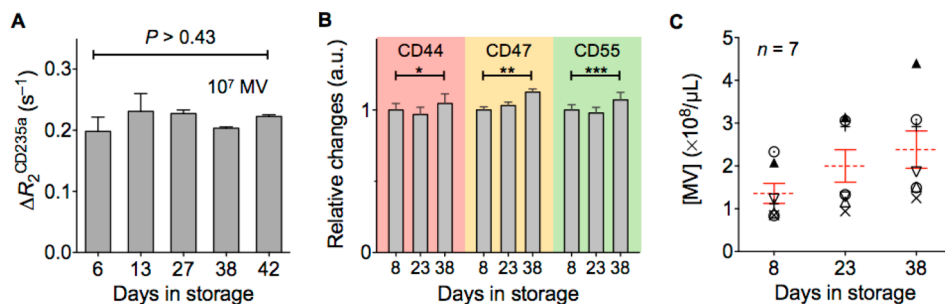


**Figure 3.** Temporal changes of MVs in pRBC units. (A) The MV concentration ([MV]) in a pRBC unit increased over time, as measured by  $\mu\text{NMR}$  (Figure S4A). When  $\Delta R_2^{\text{CD235a}}$  values were normalized against MV counts, the microvesicular expression of CD235a was statistically identical ( $P > 0.43$ ) regardless of storage time. The observed increase in  $\Delta R_2^{\text{CD235a}}$  could thus be attributed to an increase in MV counts, not to the change of CD235a expression on MVs. (B) The expression levels of other surface markers (CD44, CD47, CD55) also showed little change over initial values. These results (shown in panels A and B) could be used as evidence that a homogeneous population of MVs are formed with blood aging.  $*P > 0.48$ ;  $**P > 0.15$ ;  $***P > 0.17$ . (C) The [MV] of different pRBC units ( $n = 7$ ) was monitored using the developed platform. In all units, the [MV] increased linearly with storage time. However, initial [MV] values and their temporal changes exhibited significant variability across different units. Red lines indicate mean  $\pm$  SEM.

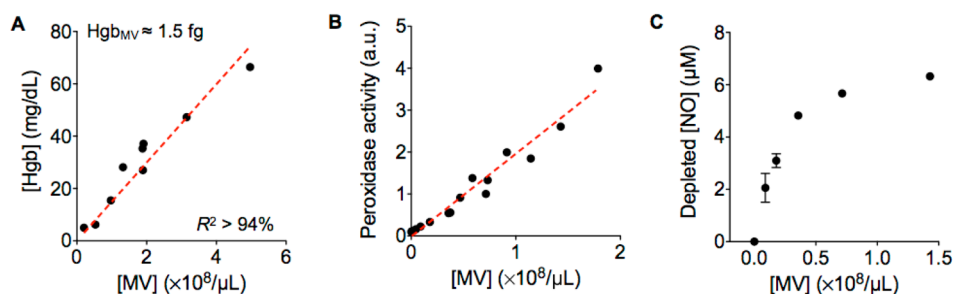


**Figure 4.** Hemoglobin (Hgb) in erythrocyte-derived MVs. (A) MVs from different blood units were assayed to determine their Hgb content. Average Hgb per MV was determined as  $\sim 1.5$  fg. (B) MVs displayed peroxidase-like activity, namely by exerting oxidative stress. (C) MVs also showed the capacity for scavenging nitric oxide (NO), a critical vasodilator. The results from (B) and (C) thus confirmed that MV-borne Hgb retains similar characteristics to cell-free Hgb.

for HRP, would be readily oxidized by MVs. Indeed, MVs showed concentration dependent peroxidase-like activity (Figure 4B), confirming their capacity for ROS generation. An inhibition assay was also employed to test the extent of NO depletion by MVs. NO in aqueous buffer typically undergoes rapid auto-oxidation to form nitrite ( $\text{NO}_2^-$ ):  $4\text{NO} + \text{O}_2 + 2\text{H}_2\text{O} \rightarrow 4\text{NO}_2^- + 4\text{H}^+$ .<sup>32</sup> Spontaneous  $\text{NO}_2^-$  production, however, could be inhibited by MV-derived Hgb *via* the following NO scavenging reactions:  $\text{Hb} + \text{NO} \rightarrow \text{HbNO}$ ;  $\text{HbO}_2(\text{Fe}^{2+}) + \text{NO} \rightarrow \text{MetHb}(\text{Fe}^{3+}) + \text{NO}_3^-$  (MetHb, methemoglobin). By then measuring the level of  $\text{NO}_2^-$  concentration, we could confirm the level of NO consumption by MVs (Figure 4C).

## CONCLUSION

Despite growing evidence describing increased risk of adverse effects with transfusion of older blood units, there is currently no standard test capable of objectively measuring the quality of stored blood units. In the current study, we addressed this need by identifying erythrocyte-derived MVs as a promising marker for monitoring blood aging. In stored blood, homogeneous MV populations were observed to increase over time; both the initial MV level and its temporal changes were observed to vary across blood samples, which

made it necessary to test individual blood over time. Importantly, we verified that MVs, like cell-free hemoglobin, have the potential to cause vascular damages through the generation of reactive oxygen species and the consumption of nitric oxide (vasodilator).

To facilitate MV analyses, we implemented a new analytical platform by combining microfluidics with magnetic detection. Although the platform lacks the capacity to resolve individual MVs, it can rapidly quantify MV concentrations as well as detect average expression of target biomarkers. Furthermore, the platform enables efficient isolation of nanoscale MVs directly from stored blood units, and allows for their detection using minimal sample purification steps. These advantages, combined with the portability of the  $\mu\text{NMR}$  system (*i.e.*, no bulky instrumentation),<sup>17</sup> render the technology poised for point-of-care testing on blood products.

Going forward, we envision that the developed technology could have broad diagnostic value. By facilitating rapid and quantitative molecular analyses of MVs from various cellular origins across disease states, this technology could promote early detection and treatment response monitoring. In turn, the expanded set of cellular and molecular information attained from individual patients could inform personalized medicine strategies.

## EXPERIMENTAL SECTION

**Packed Red Blood Cell (pRBC) Units and MV Preparation.** pRBC units were obtained from the Massachusetts General Hospital (MGH) Blood Bank (Boston, MA). The units were preserved in Adsol solution and were returned to the blood bank after an attempted transfusion (within 30 min of leaving the blood bank). Throughout this time, all units were stored at 4 °C. Portions of blood, drawn through a sterile coupler and 25G needle, were processed by the microfluidic devices. As a comparison, MVs were also isolated by serial centrifugations. For this, blood samples were initially centrifuged twice at 2000g for 15 min to remove cellular components before being centrifuged twice again at 100 000g for 70 min to obtain the MVs. The MV pellets were then reconstituted in phosphate buffered saline (PBS) solution.

**Microfluidic Device Fabrication and Assembly.** The microfluidic devices were fabricated by stacking three layers of polydimethylsiloxane (PDMS; Dow Corning) on a glass slide. The cast

molds for the bottom and top layers were prepared by patterning epoxy-based SU8-3050 photoresist (Microchem) *via* conventional photolithography. A filter PDMS block was also prepared separately by sandwiching a membrane filter (400 nm pore diameter; Nuclepore, Whatman) with two 1 mm-thick PDMS slabs ( $5 \times 5 \text{ mm}^2$ ). This filter was used to capture microbeads during MV-labeling. The channel patterns and site-locators for torque-actuated valves were contained within the bottom PDMS layer (thickness, 1 mm), while additional fluidic channels were contained within the top PDMS layer (thickness 1 mm). Initially, the PDMS filter block and bolt-nut pairs (#4-40) were aligned and glued on top of the bottom layer. Uncured PDMS polymer was then poured over the assembly, forming the intermediate layer (final thickness, 2 mm). After the polymer had cured, the top PDMS layer was irreversibly bonded to the intermediate layer *via* oxygen plasma treatment. Inlet and outlet reservoirs were punched out, and the assembled device was finally bonded irreversibly to a glass slide.

For isolating MVs from the pRBC units, a replaceable Vivid Plasma Separation membrane filter (GR grade, Pall Life Sciences), cut into a disk-shape (diameter, 25 mm), was used. A capillary guide (diameter, 25 mm), which collects filtrate, was also patterned onto polyethylene terephthalate (PET) film (thickness, 132  $\mu\text{m}$ ) via laser cutting. This filter set was then mounted onto the inlet of the microfluidic device using a pair of ring magnets (K&J Magnetics) as a clamp.

**Modification of Microbeads for MV Capture.** Antibody coated capture beads were prepared by incubating streptavidin-coated polystyrene particles (1  $\mu\text{m}$  in diameter, Spherotech, SVP-10-5) with biotinylated capture antibody for 30 min before washing in PBS.

**Tetrazine (TZ) Modification of Magnetic Nanoparticles (MNPs).** Amine-terminated cross-linked iron oxide (CLIO) nanoparticles with a hydrodynamic diameter of 21 nm were used for all magnetic labeling. Amino-CLIO was then modified with 2,5-dioxopyrrolidin-1-yl 5-(4-(1,2,4,5-tetrazin-3-yl)benzylamino)-5-oxopentanoate (TZ-NHS) to create CLIO-TZ.<sup>19</sup> The reaction was performed in 200-fold excess TZ-NHS relative to amino-CLIO, and proceeded in PBS containing 0.1 M sodium bicarbonate for 3 h at room temperature. Following conjugation, excess TZ-NHS was removed using Sephadex G-50 columns (GE Healthcare).

**Antibody Modification with *trans*-Cyclooctene (TCO).** Antibodies were modified with (*E*)-cyclooct-4-enyl 2,5-dioxopyrrolidin-1-yl carbonate (TCO-NHS), as previously reported.<sup>19</sup> Each antibody was buffer-exchanged into PBS (pH 8.0) using 2 mL Zeba desalting columns (Thermo Fisher). Purified antibodies were then reacted with 1000-fold excess TCO-NHS in 10% dimethylformamide for 3 h at room temperature. TCO conjugated antibodies were subsequently purified by buffer exchange into PBS, and their concentrations were determined by absorbance measurements. The following antibodies were used in this study: human CD235a (Clone GA-R2, BD), CD55 (Clone JS11, Biologend), CD47 (Clone CC2C6, Biologend), CD44 (Clone IM7, Biologend).

**MV Labeling with the Microfluidic Cartridge.** Samples (100  $\mu\text{L}$ ) from each pRBC unit were loaded into the inlets of the fluidic cartridge. Negative pressure was then applied to collect MVs in the reservoir (see Figure S2 for details of device operation). Following MV collection, the MNP-labeling procedure was performed by repeating the following three-step sequence: reagent addition, mixing (binding), and re-collection. For example, to capture MVs on microbeads, the following steps were performed: (1) 1- $\mu\text{m}$  microbeads modified with capture antibodies (CD235a) were introduced into the reservoir containing the MVs. In a 100  $\mu\text{L}$  sample volume, the MV and microbead concentrations were  $10^8$  to  $10^9$  MVs and  $5 \times 10^7$  beads, respectively. (2) The mixture of MVs and microbeads was then flowed through the extended mixing channel. (3) At the end of the mixing channel, the MV-bound beads (MV-beads) were retained by an in-line membrane filter (pore-size: 400 nm). Buffer solution was used to wash. (4) Reverse flow from the buffer inlet was then applied to release and recollect the MV-beads in the reservoir. Similar steps were likewise performed following the addition of mAb-TCO into the reservoir, which resulted in mAb-TCO-MV-beads. Repeating the steps with MNP-TZ ultimately resulted in MVs labeled with MNPs (see Supplementary Methods for illustration of fluidic operation). The entire process could be completed within 30 min.

**Micronuclear Magnetic Resonance ( $\mu\text{NMR}$ ) Measurement.**  $\mu\text{NMR}$  measurements were performed using a previously described miniaturized NMR relaxometer.<sup>17</sup> The operating magnetic field, generated by a portable permanent magnet, was 0.5 T. The transverse relaxation rate ( $R_2$ ) was measured on 2- $\mu\text{L}$  sample volumes using Carr–Purcell–Meiboom–Gill pulse sequences with the following parameters: echo time, 4 ms; repetition time, 1 s; the number of 180° pulses per scan, 50; the number of scans, 8. All measurements were performed in triplicate, and the data are displayed as mean  $\pm$  SEM.

**Comparative Assays.** For ELISA measurements, purified MVs were initially captured in antibody coated polystyrene 96-wells before subsequent labeling with biotinylated antibody and streptavidin–HRP. Following the addition of substrate, chemiluminescence was measured (Safire, Tecan). MV concentrations

were also measured by NTA (NanoSight, LM10) as per the manufacturer's instructions.

**MV Toxicity Assays.** MV samples were prepared by processing pRBC units with the developed microfluidic cartridge. MV concentrations were then estimated following  $\mu\text{NMR}$  detection of CD235a. (1) *Hgb measurement*: MVs were reacted with Drabkin's reagent (Sigma) to convert Hgb to cyanomethemoglobin, before measuring absorbance (540 nm). (2) *Peroxidase activity*: TMB and peroxidase (Thermo-Fisher) were mixed in equal amounts and the mixture distributed into a 96-well plate. PBS solution containing MVs of different concentrations was then added to each well. Absorbance at 370 nm was measured to estimate peroxidase activity. (3) *NO depletion*: MVs of varying concentration in PBS were added to a 96-well plate containing freshly prepared 50 mM 1,1-diethyl-2-hydroxy-2-nitrosodiazine (DEA NONOate). The mixture was incubated on ice for 20 min. Nitrite concentrations were then measured using Griess reagent as per the manufacturer's protocol (Promega).

**Conflict of Interest:** The authors declare no competing financial interest.

**Acknowledgment.** The authors thank Y. Fisher-Jeffes for review of the manuscript; N. Sergeev for synthesis of MNPs; H. Chung, and J. Higgins for many helpful discussions; X. Breakefield and L. Balaj for the use of NTA. This work was supported in part by an HHMI Medical Research Fellows Program grant (J.R.), and by the following National Institute of Health Grants: R01-HL113156 (H.L.), R01-EB010011 (R.W.), R01-EB00462605A1 (R.W.) and NHLBI contract HHSN268201000044C (R.W.).

**Supporting Information Available:** Membrane filter characterization; microfluidic device for MV capture and labeling; MV detection limit determined by  $\mu\text{NMR}$ ; temporal changes in MVs. This material is available free of charge via the Internet at <http://pubs.acs.org>.

## REFERENCES AND NOTES

1. Thery, C.; Ostrowski, M.; Segura, E. Membrane Vesicles as Conveyors of Immune Responses. *Nat. Rev. Immunol.* **2009**, *9*, 581–593.
2. Wolf, P. The Nature and Significance of Platelet Products in Human Plasma. *Br. J. Haematol.* **1967**, *13*, 269–288.
3. Shao, H.; Chung, J.; Balaj, L.; Charest, A.; Bigner, D. D.; Carter, B. S.; Hochberg, F. H.; Breakefield, X. O.; Weissleder, R.; Lee, H. Protein Typing of Circulating Microvesicles Allows Real-Time Monitoring of Glioblastoma Therapy. *Nat. Med.* **2012**, *18*, 1835–1840.
4. Balaj, L.; Lessard, R.; Dai, L.; Cho, Y. J.; Pomeroy, S. L.; Breakefield, X. O.; Skog, J. Tumour Microvesicles Contain Retrotransposon Elements and Amplified Oncogene Sequences. *Nat. Commun.* **2011**, *2*, 180.
5. Skog, J.; Wurdinger, T.; van Rijn, S.; Meijer, D. H.; Gainche, L.; Sena-Esteves, M.; Curry, W. T. J.; Carter, B. S.; Krichevsky, A. M.; Breakefield, X. O. Glioblastoma Microvesicles Transport RNA and Proteins That Promote Tumour Growth and Provide Diagnostic Biomarkers. *Nat. Cell Biol.* **2008**, *10*, 1470–1476.
6. Bosman, G. J.; Werre, J. M.; Willekens, F. L.; Novotny, V. M. Erythrocyte Ageing *in Vivo* and *in Vitro*: Structural Aspects and Implications for Transfusion. *Transfus. Med.* **2008**, *18*, 335–347.
7. Willekens, F. L.; Werre, J. M.; Groenen-Dopp, Y. A.; Roerdinkholder-Stoelwinder, B.; de Pauw, B.; Bosman, G. J. Erythrocyte Vesiculation: A Self-Protective Mechanism?. *Br. J. Haematol.* **2008**, *141*, 549–556.
8. Tissot, J.-D.; Rubin, O.; Canellini, G. Analysis and Clinical Relevance of Microparticles from Red Blood Cells. *Curr. Opin. Hematol.* **2010**, *17*, 571–577.
9. Zallen, G.; Offner, P. J.; Moore, E. E.; Blackwell, J.; Ciesla, D. J.; Gabriel, J.; Denny, C.; Silliman, C. C. Age of Transfused Blood is an Independent Risk Factor for Postinjury Multiple Organ Failure. *Am. J. Surg.* **1999**, *178*, 570–572.
10. Moore, F. A.; Moore, E. E.; Sauaia, A. Blood Transfusion. An Independent Risk Factor for Postinjury Multiple Organ Failure. *Arch. Surg.* **1997**, *132*, 620–625.

11. Napolitano, L. M.; Kurek, S.; Luchette, F.; Corwin, H. L.; Barie, P. S.; Tisherman, S. A.; Hebert, P. C.; Anderson, G. L.; Bard, M. R.; Bromber, W.; *et al.* Clinical Practice Guideline: Red Blood Cell Transfusion in Adult Trauma and Critical Care. *Crit. Care Med.* **2009**, *37*, 3124–3157.
12. Koch, C. G.; Li, L.; Sessler, D. I.; Figueroa, P.; Hoeltge, G. A.; Mihaljevic, T.; Blackstone, E. H. Duration of Red-Cell Storage and Complications after Cardiac Surgery. *N. Engl. J. Med.* **2008**, *358*, 1229–1239.
13. Freyssinet, J. M.; Toti, F. Membrane Microparticle Determination: At Least Seeing What's Being Sized!. *J. Thromb. Haemost.* **2010**, *8*, 311–314.
14. Rubin, O.; Crettaz, D.; Tissot, J. D.; Lion, N. Pre-analytical and Methodological Challenges in Red Blood Cell Microparticle Proteomics. *Talanta* **2010**, *82*, 1–8.
15. Rubin, O.; Crettaz, D.; Canellini, G.; Tissot, J. D.; Lion, N. Microparticles in Stored Red Blood Cells: An Approach Using Flow Cytometry and Proteomic Tools. *Vox Sang.* **2008**, *95*, 288–297.
16. Lawrie, A. S.; Albanyan, A.; Cardigan, R. A.; Mackie, I. J.; Harrison, P. Microparticle Sizing By Dynamic Light Scattering in Fresh-Frozen Plasma. *Vox Sang.* **2009**, *96*, 206–212.
17. Issadore, D.; Min, C.; Liong, M.; Chung, J.; Weissleder, R.; Lee, H. Miniature Magnetic Resonance System for Point-of-Care Diagnostics. *Lab Chip* **2011**, *11*, 2282–2287.
18. Thery, C.; Amigorena, S.; Raposo, G.; Clayton, A. Isolation and Characterization of Exosomes From Cell Culture Supernatants and Biological Fluids. *Curr. Protoc. Cell Biol.* **2006**, Chapter 3, No. Unit 3.22.
19. Haun, J. B.; Devaraj, N. K.; Hilderbrand, S. A.; Lee, H.; Weissleder, R. Bioorthogonal Chemistry Amplifies Nanoparticle Binding and Enhances the Sensitivity of Cell Detection. *Nat. Nanotechnol.* **2010**, *5*, 660–665.
20. Peterson, V. M.; Castro, C. M.; Lee, H.; Weissleder, R. Orthogonal Amplification of Nanoparticles for Improved Diagnostic Sensing. *ACS Nano* **2012**, *6*, 3506–3513.
21. Shao, H.; Yoon, T. J.; Liong, M.; Weissleder, R.; Lee, H. Magnetic Nanoparticles for Biomedical NMR-Based Diagnostics. *Beilstein J. Nanotechnol.* **2010**, *1*, 142–154.
22. Min, C.; Shao, H.; Liong, M.; Yoon, T. J.; Weissleder, R.; Lee, H. Mechanism of Magnetic Relaxation Switching Sensing. *ACS Nano* **2012**, *6*, 6821–6828.
23. Chasis, J. A.; Mohandas, N. Red Blood Cell Glycophorins. *Blood* **1992**, *80*, 1869–1879.
24. Zennadi, R.; Chien, A.; Xu, K.; Batchvarova, M.; Telen, M. J. Sick Red Cells Induce Adhesion of Lymphocytes and Monocytes to Endothelium. *Blood* **2008**, *112*, 3474–3483.
25. Oldenburg, P. A.; Zheleznyak, A.; Fang, Y. F.; Lagenaur, C. F.; Gresham, H. D.; Lindberg, F. P. Role of Cd47 as a Marker of Self on Red Blood Cells. *Science* **2000**, *288*, 2051–2054.
26. Oldenburg, P. A. Role of Cd47 in Erythroid Cells and in Autoimmunity. *Leuk. Lymphoma* **2004**, *45*, 1319–1327.
27. Donadee, C.; Raat, N. J. H.; Kanas, T.; Tejero, J.; Lee, J. S.; Kelley, E. E.; Zhao, X.; Liu, C.; Reynolds, H.; Azarov, I.; *et al.* Nitric Oxide Scavenging By Red Blood Cell Microparticles and Cell-Free Hemoglobin as a Mechanism for the Red Cell Storage Lesion. *Circulation* **2011**, *124*, 465–476.
28. Gladwin, M. T.; Kim-Shapiro, D. B. Storage Lesion in Banked Blood Due to Hemolysis-Dependent Disruption of Nitric Oxide Homeostasis. *Curr. Opin. Hematol.* **2009**, *16*, 515–523.
29. Grimshaw, K.; Sahler, J.; Spinelli, S. L.; Phipps, R. P.; Blumberg, N. New Frontiers in Transfusion Biology: Identification and Significance of Mediators of Morbidity and Mortality in Stored Red Blood Cells. *Transfusion* **2011**, *51*, 874–880.
30. Ballas, S. K.; Marcolina, M. J. Hyperhemolysis during the Evolution of Uncomplicated Acute Painful Episodes in Patients with Sick Cell Anemia. *Transfusion* **2006**, *46*, 105–110.
31. Takahashi, Y.; McCoy, J. P. J.; Carvallo, C.; Rivera, C.; Igarashi, T.; Srinivasan, R.; Young, N. S.; Childs, R. W. *In Vitro* and *In Vivo* Evidence of PNH Cell Sensitivity to Immune Attack after Nonmyeloablative Allogeneic Hematopoietic Cell Transplantation. *Blood* **2004**, *103*, 1383–1390.
32. Ford, P. C.; Wink, D. A.; Stanbury, D. M. Autoxidation Kinetics of Aqueous Nitric Oxide. *FEBS Lett.* **1993**, *326*, 1–3.